

Pseudo-FIMP dark matter in presence of a SIMP

Subhaditya Bhattacharya,^a Dipankar Pradhan,^a Jahaan Thakkar.^{a,b}

^a*Department of Physics, Indian Institute of Technology Guwahati,
North Guwahati, Assam-781039, India,*

^b*Department of Theoretical Physics, Tata Institute of Fundamental Research,
Mumbai, Maharashtra-400005, India,*

E-mail: subhab@iitg.ac.in, d.pradhan@iitg.ac.in,
jahaan.thakkar@tifr.res.in

ABSTRACT: Pseudo-feebly Interacting Massive Particle (pFIMP) has been postulated in two component dark matter (DM) scenarios, where it has feeble interaction with the visible sector, but sizeable one with a thermal bath partner. In this work, we study the possibility and dynamics of pFIMP in presence of a Strongly Interacting Massive Particle (SIMP), which is well known to solve too-big-to-fail and core-vs-cusp problems. Our analysis is primarily model-independent via solving coupled Boltzmann equations, with negligible DM-DM conversion adhering to pure SIMP-FIMP limit, and then with larger DM-DM conversion rate pertaining to SIMP-pFIMP limit. We also illustrate the simplest model yielding pFIMP-SIMP set-up having two scalars stabilised under $\mathbb{Z}_2 \otimes \mathbb{Z}_3$ symmetry, and explore the accessible parameter space after addressing relic density, unitarity, self interaction constraints etc. pFIMP detectability is limited in such circumstances, but possible via a thermal DM loop when the SIMP has a visible sector interaction via light mediator.

KEYWORDS: Models for Dark Matter, Particle Nature of Dark Matter, Specific BSM Phenomenology, Dark Matter at Colliders.

Contents

1	Introduction	1
2	A brief discussion on the simplest SIMP model	2
3	pFIMP in presence of a SIMP: model independent analysis	6
4	A model example of pFIMP-SIMP	9
4.1	Solution of coupled Boltzmann Equation and relic density	9
4.2	Constraints on the model parameter space	11
4.3	Detection possibility	13
5	Summary and conclusions	14
A	The semi-analytical solution of a SIMP	15
B	Possible Feynman diagrams related to DM phenomenology	17
C	Dark Matter self-interaction	19
D	DM Kinetic equilibration	20

1 Introduction

Our universe is full of mysteries. The presence of a non-luminous matter component, known as Dark Matter (DM) [1, 2] is one of them. Different kinds of astrophysical and cosmological observations, like Galaxy rotation curves [3], Bullet Cluster [4], CMBR anisotropic spectrum [5] suggest that DM is present and possesses 26.8% of the energy budget of the Universe and this gives rise to one of the most important observables related to DM, called the relic density, expressed as $\Omega_{\text{DM}}h^2 = 0.1200 \pm 0.0012$ [6], where $\Omega = \rho/\rho_c$ is cosmological density and h is reduced Hubble constant.

What constitutes the DM is a key question, which has involved a lot of researches and possibilities so far. Particle DM has been very popular since it can judiciously explain almost all the observations related to DM. However, none of the observations can pinpoint what kind of particle it is, although some broad characteristics like electromagnetic charge neutrality, massiveness and stability at the scale of Universe’s life time are assigned to them. Further debate erupts on the question whether the DM is composed of a single type of particle or have different particles of different nature, adhering to the broad characteristics of DM. Again, the possibilities here are infinite and the only relevant constraint comes from the Bullet cluster observation, which restricts the DM-DM self-interaction [7]. One thing

we know for sure, that Standard Model (SM) of particle physics do not contain any DM and requires extension to accommodate one (or more) DM, protected by a symmetry different from that of SM gauge symmetries.

DM characteristics mainly depend on its production mechanism. There are two possibilities (broadly) depending on whether it was in thermal bath during reheating or not. Those which were in equilibrium with bath and freezes out at some point with expanding universe are called thermal DM, and those which were not in equilibrium and produced via out-of-equilibrium processes to freeze in, are called non-thermal ones. The most popular thermal DM candidates are weakly interacting massive particle (WIMP)[8–13] and strongly interacting massive particle (SIMP) [14–21], while a well studied non-thermal possibility gives rise to feebly interacting massive particle (FIMP) [22–27] type of DM. Multipartite DM can be constituted by any combination of them. The most studied frameworks involve similar DM components, like WIMP-WIMP [28, 29], FIMP-FIMP [30, 31], and SIMP-SIMP [32, 33]. WIMP-FIMP [34, 35] combination is possible when the interaction between DM components is also feeble. However, if we have sizeable interaction between the DM components, then it gives rise to an interesting possibility of a pseudo FIMP (pFIMP) [36–38] type DM. How? Then FIMP, in spite of having feeble interaction with the visible sector, reaches thermal equilibrium thanks to the large conversion with the WIMP partner, and is called pseudo-FIMP (pFIMP). pFIMP then undergoes freeze-out similar to WIMP. However the freeze-out characteristics depend on the WIMP partner, making it a special/different DM component.

We wish to take the study of pFIMP one step ahead. We show here how pFIMP can be realised in presence of a SIMP like DM component. The freeze out characteristics of pFIMP then depends very much on those of its SIMP partner. We establish this in a model independent analysis via solving coupled Boltzmann Equations, so that it is applicable to any kind of pFIMP-SIMP combination, immaterial to their particle properties. Second, we establish the same via a concrete model example involving two scalar fields, one real, and the other complex, stabilized by $\mathbb{Z}_2 \otimes \mathbb{Z}_3$ symmetry. This is arguably the simplest scenario yielding pFIMP-SIMP model. The search strategies for DM known so far, like direct detection (DD), indirect detection (ID), or collider searches are difficult to reveal such DM combinations unless the SIMP is accessible to the detector via light mediator.

This article is organized as follows: sec. 2 provides a brief discussion on a single component SIMP, sec. 3 explores the dynamics and phenomenology of pFIMP in a model-independent manner, and sec. 4 presents a model example. Finally, we summarize in sec. 5. Appendices A, B, C, and D provide additional details that were omitted in the main text.

2 A brief discussion on the simplest SIMP model

For WIMP, the DM freeze out depends on the thermal average of annihilation cross-section ($2_{\text{DM}} \rightarrow 2_{\text{SM}}$). For SIMP, DM freeze out (FO) occur mainly via self-interaction like $3_{\text{DM}} \rightarrow 2_{\text{DM}}$ [19] (or $4_{\text{DM}} \rightarrow 2_{\text{DM}}$ [39]) annihilations within the dark sector, while $2_{\text{DM}} \rightarrow 2_{\text{SM}}$ annihilation is suppressed. The equilibration of SIMP to thermal bath is main-

tained by scattering with SM particles ($\text{DM}+\text{SM} \rightarrow \text{DM}+\text{SM}$), the rate of which is given by $\Gamma = n_{eq}\langle\sigma v\rangle$, which can be larger than the Hubble expansion rate (H) due to the large relativistic SM number density (n_{eq}), in spite of the small annihilation cross-section to SM. The hierarchy of interactions that keeps SIMP in thermal bath without heating up the dark sector is therefore,

$$\Gamma_{\text{DM}+\text{SM}\rightarrow\text{DM}+\text{SM}} \gtrsim \Gamma_{3_{\text{DM}}\rightarrow 2_{\text{DM}}} \gtrsim \Gamma_{2_{\text{DM}}\rightarrow 2_{\text{SM}}}. \quad (2.1)$$

However for the five body ($3_{\text{DM}} \rightarrow 2_{\text{DM}}$) or six body depletion process ($4_{\text{DM}} \rightarrow 2_{\text{DM}}$) that governs SIMP freeze out, the DM mass needs to be adjusted to account for the larger phase space volume and is of the order of MeV to address correct relic density. The coupling for such a number-changing process within the dark sector must also be significantly large to take into account of the phase space suppression. Hence, such a class of DM is called Strongly Interacting Massive Particle (SIMP) [16, 19, 39–41]. We may stress here again that strong interaction here doesn't refer to strong interaction between dark and SM particles, but it is within the dark sector particles.

Concerning SIMP, the simplest possibility emerges when we take a complex scalar singlet (χ), which transforms under \mathbb{Z}_3 symmetry. Corresponding Lagrangian is [19],

$$\mathcal{L} = \mathcal{L}_{\text{SM}} + |\partial_\mu \chi|^2 - m_\chi^2 |\chi|^2 - \lambda_\chi |\chi|^4 - \lambda_{\chi H} \left(H^\dagger H - \frac{v^2}{2} \right) |\chi|^2 - \frac{\mu_3}{2} (\chi^3 + \chi^{*3}), \quad (2.2)$$

where $\mu_3, \lambda_\chi, \lambda_{\chi H} > 0$. Note here that the above Lagrangian is valid for any charge of χ or χ^* as ω, ω^2 , where $\omega^3 = 1$.

• Unitarity and Perturbativity

Using the unitarity of the S-matrix, *i.e.* the optical theorem, the maximum value of the inelastic cross-section for an identical particle is [21, 42–44],

$$\left\langle \sigma_{k \rightarrow 2} v_{rel}^{k-1} \right\rangle_{\text{max}} = \sum_l (2l+1) \frac{2^{\frac{3k-2}{2}} (\pi x)^{\frac{3k-5}{2}}}{g_{\text{DM}}^{k-2} m_{\text{DM}}^{3k-4}}. \quad (2.3)$$

and for non-identical particles in non-relativistic approximation with s-wave contribution [45],

$$\left\langle \sigma_{k \rightarrow 2} v_{rel}^{k-1} \right\rangle \leq 2^{(3k-1)/2} (T/\pi)^{(5-3k)/2} S_k \frac{g_4 g_5}{g_1 \dots g_k} \left(\frac{m_1 + \dots + m_k}{m_1 \dots m_k} \right)^{3/2}, \quad (2.4)$$

where S_k is the symmetry factor associated with identical particles in the initial state, and g_k counts the degrees of freedom of i^{th} particle. In our case maximum value of $3\text{DM} \rightarrow 2\text{DM}$ annihilation are,

$$\left\langle \sigma_{\chi\chi\chi \rightarrow \chi\chi^*} v_{rel}^2 \right\rangle \leq \frac{48\sqrt{3}\pi^2}{m_\chi^3 T^2} 3! \quad \text{and} \quad \left\langle \sigma_{\chi\chi\chi^* \rightarrow \chi^* \chi^*} v_{rel}^2 \right\rangle \leq \frac{48\sqrt{3}\pi^2}{m_\chi^3 T^2} 2!. \quad (2.5)$$

However, these constraints are very mild for MeV scale DMs. The unitarity bound in the infinite scattering energy limit is given by [46–50],

$$|\lambda_{\chi H}| \leq 8\pi, \quad |\lambda_\chi| \leq 4\pi. \quad (2.6)$$

The perturbative bound for this model is given by [19, 33],

$$|\lambda_{\chi H}| \leq 4\pi, \quad |\lambda_\chi| \leq \pi. \quad (2.7)$$

- **Vacuum Stability**

The necessary condition to stabilise the potential (2.2) is,

$$\lambda_H > 0, \quad \lambda_\chi > 0, \quad \lambda_{\chi H} + 2\sqrt{\lambda_\chi \lambda_H} > 0. \quad (2.8)$$

The maximal allowed value of the cubic parameter μ_3 is approximately equal to $\mu_3|_{\max} \approx 2\sqrt{2}\sqrt{\lambda_\chi/\delta} m_\chi$ where dimensionless parameter δ parameterises the energy difference of vacua [51]. For $\delta = 2$, the \mathbb{Z}_3 breaking minimum is approximately degenerate with the SM minimum and gives the absolute stability bound [47, 50].

- **Kinetic equilibrium**

The dominating FO process for SIMP is $3_{\text{DM}} \rightarrow 2_{\text{DM}}$, which converts some fraction of DM (SIMP) mass into dark matter kinetic energy and gets distributed among themselves and the scattering with SM bath particles transfer energy to the thermal bath, otherwise this will heat up the dark sector core and violates the astrophysical constraints derived from the structure formation [52]. The kinetic equilibrium should be maintained between DM and SM bath minimally up to the freeze out of χ so that $T_{\text{SM}} = T_{\text{DM}}$. The required condition to achieve this is $\langle \Gamma_{\chi \text{ SM} \rightarrow \chi \text{ SM}} \rangle_{T=T_\chi^{\text{FO}}} \gtrsim \mathcal{H}(T_\chi^{\text{FO}})$ and is one of the most important conditions for SIMP. DM can scatter with relativistic SM fermions, which is in thermal equilibrium during FO. As the relativistic fermions (f) are abundant in the radiation-dominated era, the scattering process $\chi f \rightarrow \chi f$ is fast enough to keep dark and the visible sector in kinetic equilibrium during FO, respecting $T_{\text{DM}} = T_{\text{SM}}$ [17, 41, 53]. We have estimated a bound on the portal coupling ($\lambda_{\chi H}$) for a sample of DM mass (m_χ) in Appendix D to maintain kinetic equilibrium. Another way to achieve the kinetic equilibrium between two sectors is to extend the dark sector by introducing a relativistic new particle during FO [54]. However, if the dark sector temperature is much less than the SM bath temperature, these two sectors can never reach kinetic equilibrium [39, 55].

- **Dark matter self scattering**

As SIMP type DM has sizeable self-interaction, which helps to solve the small-scale problems [17, 56] but is constrained by several observational constraints like,

- ★ Bullet cluster [57–59]: $\frac{\sigma_{\text{self}}}{m_{\text{DM}}} \lesssim 1 \text{ cm}^2 \text{ gm}^{-1}$.
- ★ Abell cluster [60]: $1 \text{ cm}^2 \text{ gm}^{-1} \lesssim \frac{\sigma_{\text{self}}}{m_{\text{DM}}} \lesssim 3 \text{ cm}^2 \text{ gm}^{-1}$.

A similar kind of bound is also available from cosmological simulation on self-interacting DM in galaxy cluster [61, 62].

- **Dark Matter Mass limits**

BBN has a put significant constraint from different cosmological observations [63–65]. So, it is an obvious choice for DM to freeze out before BBN; *i.e.* $T_{\text{FO}} > T_{\text{BBN}} \sim 0.1 \text{ MeV}$ gives an essential constraint on the masses of thermal DM. For DM masses above 10 MeV, BBN constitutes an important probe for the annihilation cross section of DM [66, 67].

• **Boltzmann Equation**

To get the present number density of SIMP DM, we have to solve the BEQ,

$$\frac{dY_\chi}{dx} = -\frac{s}{x \mathcal{H}(x)} \left[\langle \sigma v \rangle_{\chi\chi^* \rightarrow \text{SM}} Y_\chi^2 - Y_\chi^{eq^2} + s \langle \sigma v^2 \rangle_{3\chi \rightarrow 2\chi} (Y_\chi^3 - Y_\chi^2 Y_\chi^{eq}) \right], \quad (2.9)$$

where $x = m_\chi/T$, $\mathcal{H}(x) = 1.67\sqrt{g_*^\rho} m_\chi^2 / (x^2 M_{\text{pl}})$, $s = \frac{2\pi^2}{45} g_*^s (m_\chi/x)^3$ and $g_*^{s(\rho)}$ is the entropy (matter) degrees of freedom. The total DM yield is twice Y_χ as its conjugate particle (χ^*) also has the same yield. Also note the presence of second term inside the parenthesis, absent in the WIMP, which dominates the SIMP like freeze out. A semi-analytical solution of eq. 2.9 has been shown in Appendix A and a comparison with the numerical solution to match closely.

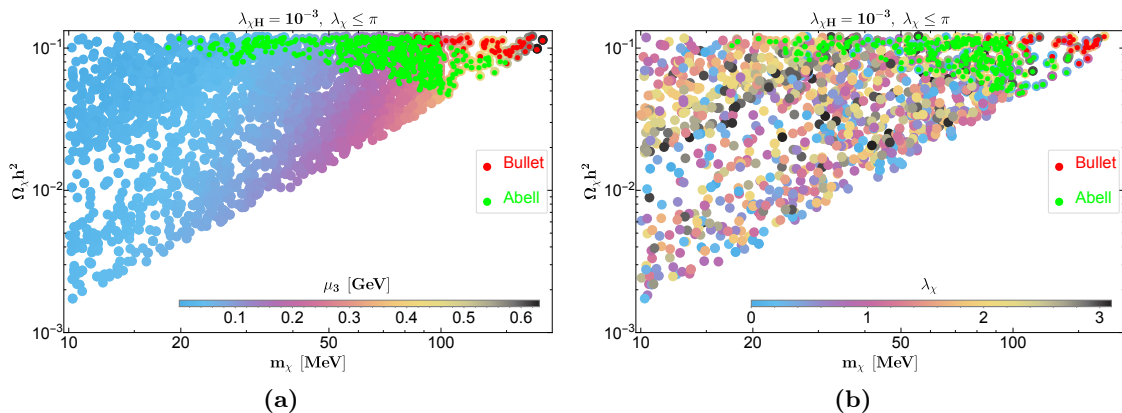


Figure 1: figs. 1a and 1b represent the relic and unitarity allowed parameter space in $m_\chi - \Omega_\chi h^2$ plane for a complex scalar SIMP (χ) described by the Lagrangian in eq. (2.2). The variation of the relevant couplings (μ_3, λ_χ) is shown in the color bar, while the ones fixed is mentioned in the figure heading. Red and green points satisfy the self interaction limits from Bullet and Abell cluster bounds, respectively.

The parameter space scan of the numerical solution of eq. 2.9 for a complex scalar SIMP (χ) described by the Lagrangian in eq. (2.2) is shown in fig. 1. In figs. 1a and 1b, we show the relic under abundant parameter space in $m_\chi - \Omega_\chi h^2$ planes and the color bar represents variation in cubic parameter μ_3 (left) and quadratic coupling λ_χ (right) within appropriate limits. The SIMP relic density is inversely proportional to the DM mass and proportional to μ_3 and λ_χ parameters, which is also reflected in figs. 1a and 1b respectively. With the enhancement of SIMP mass, DM self-annihilation cross section decreases, and the relic density is enhanced. To adjust the relic density, we have to increase the couplings within the theoretical limits. We are getting DM mass up to $m_\chi \lesssim 200$ MeV in a single-component complex scalar SIMP scenario to acquire correct relic density. The self-scattering cross-section over DM mass, eq. C.1 strongly constrains the relic density allowed parameter space. After considering all of the available theoretical and cosmological constraints, few points respect the presently available DM self-interaction bound from Bullet and Abell cluster, marked by red and green points respectively as shown in fig. 1. This

preliminary analysis helps us addressing the phenomenological distinction with the two component scenario considered later in this paper. Before concluding this section, let us furnish some of the two component DM frameworks in combination with SIMP in tab. 1 and remind that we focus on the pFIMP-SIMP combination, which was briefly mentioned in [36].

Scenario	w - s	$\Gamma_{\text{SM SM} \rightarrow \text{w w}}$	$\Gamma_{\text{SM SM} \rightarrow \text{s s}}$	$\Gamma_{\text{s s} \rightarrow \text{w w}}$	Self Annihilation
I	FIMP-SIMP	Feeble	Weak	Feeble	Weak-Strong
II	pFIMP-SIMP [this work]	Feeble	Weak	Weak	Weak-Strong
III	WIMP-SIMP	Weak	Weak	Weak/Feeble	Weak-Strong
IV	SIMP-SIMP [32, 33]	Weak	Weak	Weak/Feeble	Strong-Strong

Table 1: Generic two-component DM scenarios in the presence of a SIMP where w and s stand for two different or the same kind of dark sector particles, and $\Gamma_{i j \rightarrow k l}$ indicate the annihilation or production rate of the respective particle.

3 pFIMP in presence of a SIMP: model independent analysis

Let us briefly recapitulate the essence of pFIMP [36, 37] first. pFIMP is a kind of thermal DM, which has feeble interaction with the visible sector, but remains in equilibrium via interaction with the thermal DM partner. pFIMP therefore, can only be realised in a multicomponent DM scenario, when its partner is in thermal equilibrium. pFIMP freeze out therefore heavily depends on the partner's character, and the partner's detectability decides pFIMP's detection possibility [37].

The existence of pFIMP was demonstrated in presence of WIMP in [36, 37]. Here we show that SIMP being another kind of thermal DM, can accommodate a pFIMP DM in a multicomponent set up (the second possibility in tab. 1), with substantial interactions between them. The analysis has been done in two steps: firstly, a model-independent analysis on the pFIMP-SIMP scenario, in sec. 3, showing that the pFIMP dynamics is possible in the presence of a SIMP. Secondly, we do the same exercise for the simplest two-component real (pFIMP) and complex scalar SIMP DM model, in sec. 4. In terms of yield $Y = n/s$ the two component cBEQ becomes,

$$\frac{dY_w}{dx} = \frac{2 \mathbf{s}}{x \mathcal{H}(x)} \left[\frac{1}{\mathbf{s}} \left(Y_{\text{SM}}^{\text{eq}} - Y_{\text{SM}}^{\text{eq}} \frac{Y_w^2}{Y_w^{\text{eq}^2}} \right) \langle \Gamma \rangle_{\text{SM SM} \rightarrow \text{w w}} + \left(Y_{\text{SM}}^{\text{eq}^2} - Y_{\text{SM}}^{\text{eq}^2} \frac{Y_w^2}{Y_w^{\text{eq}^2}} \right) \langle \sigma v \rangle_{\text{SM SM} \rightarrow \text{w w}} \right. \\ \left. + \left(Y_s^2 - Y_s^{\text{eq}^2} \frac{Y_w^2}{Y_w^{\text{eq}^2}} \right) \langle \sigma v \rangle_{\text{s s} \rightarrow \text{w w}} \right], \quad (3.1)$$

$$\frac{dY_s}{dx} = -\frac{\mathbf{s}}{x \mathcal{H}(x)} \left[\left(Y_s^2 - Y_s^{\text{eq}^2} \right) \langle \sigma v \rangle_{\text{s s} \rightarrow \text{SM SM}} + \mathbf{s} \left(Y_s^3 - Y_s^2 Y_s^{\text{eq}} \right) \langle \sigma v^2 \rangle_{3\text{s} \rightarrow 2\text{s}} \right. \\ \left. + \left(Y_s^2 - Y_s^{\text{eq}^2} \frac{Y_w^2}{Y_w^{\text{eq}^2}} \right) \langle \sigma v \rangle_{\text{s s} \rightarrow \text{w w}} \right]. \quad (3.2)$$

In the above, Y_w refers to pFIMP yield, and Y_s defines SIMP yield. $\mathcal{H}(x) = 1.67\sqrt{g_*^\rho}\mu_{sw}^2/(x^2M_{\text{pl}})$, $\mathbf{s} = \frac{2\pi^2}{45}g_*^{\mathbf{s}}(\mu_{sw}/x)^3$, $Y_i^{\text{eq}} = \frac{45}{4\pi^4}\frac{g_i}{g_*}\left(\frac{m_i}{\mu_{sw}}x\right)^2K_2\left(\frac{m_i}{\mu_{sw}}x\right)$.

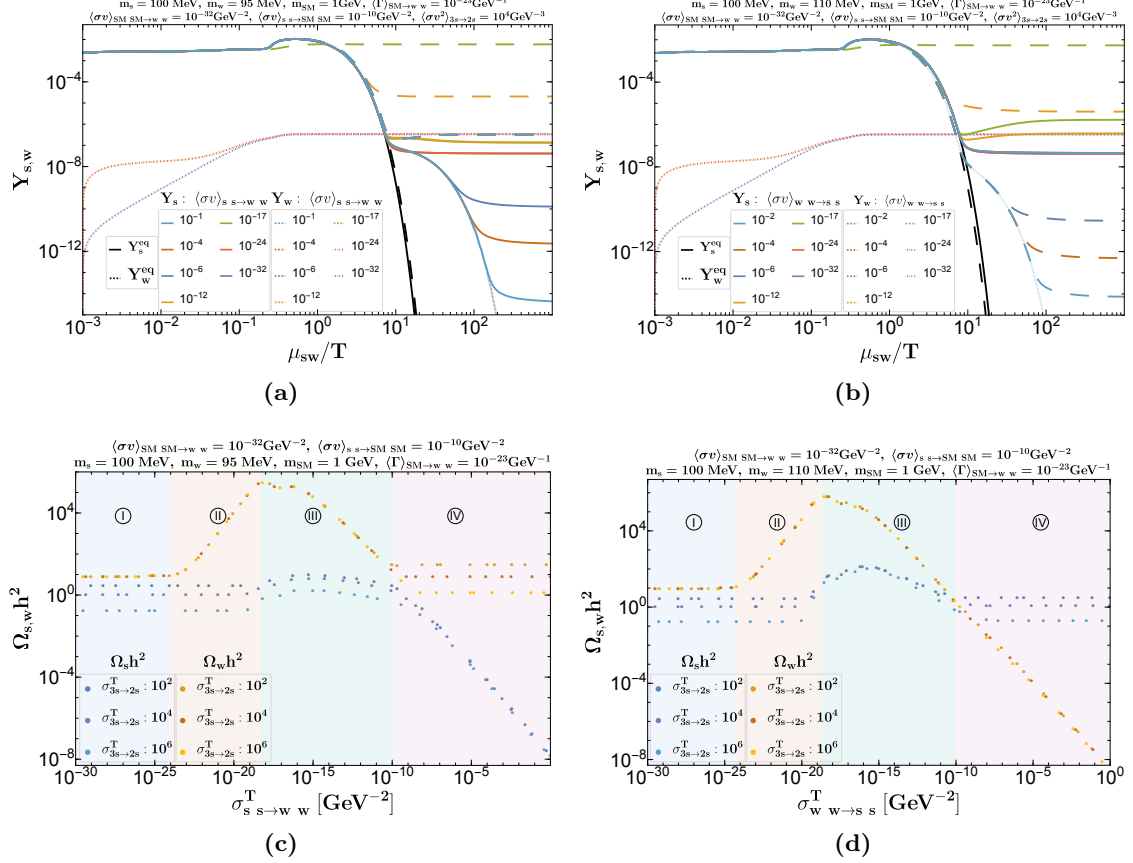


Figure 2: Solution to cBEQs 3.1, and 3.2 for pFIMP-SIMP scenario; figs. 2a, 2c represent $m_s > m_w$ case, while figs. 2b, 2d represent $m_s < m_w$ case. Figs. 2a, 2b represent the variation of DM yield with dimensionless parameter μ_{sw}/T for different values of conversion cross-section illustrated by different colored lines, solid for SIMP, dashed for pFIMP. Figs. 2c, 2d represent DM relics as a function of DM-DM conversion cross-sections. Different colored dotted lines correspond to different SIMP annihilation cross-sections as mentioned in the plot legends.

The solution of cBEQ, 3.1 and 3.2, is shown in figs. 2a, 2c for $m_w > m_s$ and in figs. 2b, 2d for $m_w < m_s$. In the top panel of fig. 2, we have varied the conversion cross-section, shown by different color thick (SIMP) and dotted/dashed (pFIMP) lines, while others m_s , m_w , $\langle\sigma v\rangle_{s\rightarrow\text{SM SM}}$, $\langle\sigma v\rangle_{w\rightarrow\text{SM SM}}$ and $\langle\sigma v^2\rangle_{3s\rightarrow 2s}$ values are kept fixed as mentioned in the figure inset. In this model-independent analysis, we have used the numerical values for thermal average cross-sections instead of a temperature-dependent functional form. The DM self-interaction constraints from different cosmological observations is yet to be considered, we do the same for model-dependent discussion.

The simplest way to explain fig. 2 by dividing the whole scenario into four regions, ① $\gamma_{sw} < \gamma_{ww}$; ② $\gamma_{ww} \lesssim \gamma_{sw} \ll \gamma_{3s\rightarrow 2s}$; ③ $\gamma_{ww} \ll \gamma_{sw} < \gamma_{3s\rightarrow 2s}$; ④ $\gamma_{3s\rightarrow 2s} \lesssim \gamma_{sw}$. We

define, $\gamma_{ww} = \langle \sigma v \rangle_{\text{SM SM} \rightarrow \text{W W}} n_{\text{SM}}^2 \equiv \langle \Gamma \rangle_{\text{SM} \rightarrow \text{W W}} n_{\text{SM}}$, $\gamma_{sw} = \langle \sigma v \rangle_{\text{S S} \rightarrow \text{W W}} n_{\text{S}}^2$ and $\gamma_{3s \rightarrow 2s} = \langle \sigma v^2 \rangle_{3s \rightarrow 2s} n_{\text{S}}^3 = \langle \sigma v^2 \rangle_{2s \rightarrow 3s} n_{\text{S}}^2$.

Region $\textcircled{\text{I}}$ shown by the light blue shaded region in figs. 2c and 2d, FIMP number density n_{W} is independent of the $\sigma_{\text{S S} \rightarrow \text{W W}}^T$ due to the negligible DM-DM conversion cross-section compared to DM production rate from SM particles. This is also visible in figs. 2a ($m_{\text{S}} > m_{\text{W}}$) and 2b ($m_{\text{S}} < m_{\text{W}}$) from blue dot-dashed lines. This scenario corresponds to a pure FIMP for Y_{W} and pure SIMP for Y_{S} .

Region $\textcircled{\text{II}}$ refers to light red regions in figs. 2c, 2d and is also represented by red dot-dashed lines in figs. 2a, 2b. In this regime, $\gamma_{ww} \lesssim \gamma_{sw} \ll \gamma_{3s \rightarrow 2s}$, SIMP number density remains unaffected due to small conversion rate compared to $\sigma_{3s \rightarrow 2s}^T$ but FIMP number density (n_{W}) is enhanced with larger conversion from SIMP, as reflected in all the four figs. This limit still represents a combination of SIMP and FIMP DMs, where FIMP production is affected by conversion from SIMP, but is mostly overabundant.

Suppose we further enhance the DM-DM conversion rate. In that case, FIMP (w) reaches thermal equilibrium and follows equilibrium before freeze out. At the same time, SIMP number density is slightly enhanced due to opening up a new annihilation or production channel, see region $\textcircled{\text{III}}$ in figs. 2c, 2d and green, yellow dashed lines in figs. 2a, 2b. After equilibration, we call the FIMP (w) as pFIMP as it has a feeble visible connection but is weakly connected with partner SIMP type DM and makes it a two-component SIMP-pFIMP scenario. With further enhancement of conversion rate (γ_{sw}), both SIMP and pFIMP number density decreases, but before freeze out, they follow a modified equilibrium distribution depending on the choice of mass hierarchy, as shown by the dotted yellow and green lines in fig. 2a. In this regime, for ($m_{\text{S}} < m_{\text{W}}$) (in fig. 2b) SIMP number density is suddenly enhanced after decoupling from the thermal bath due to the production from pFIMP, which is also seen in fig. 2c. The expression of modified equilibrium number densities that the particles acquire in fig. 2a and 2b for two hierarchies are given by eqs. 3.3 and 3.4 respectively,

$$n_{\text{W}}^{\text{eq}'} = n_{\text{W}}^{\text{eq}} \frac{n_{\text{S}}}{n_{\text{S}}^{\text{eq}}} \quad \text{for } m_{\text{W}} > m_{\text{S}}, \quad (3.3)$$

$$n_{\text{S}}^{\text{eq}'} = n_{\text{S}}^{\text{eq}} \left[\frac{\langle \sigma v \rangle_{\text{S S} \rightarrow \text{SM SM}} + \left(\frac{n_{\text{S}}^2}{n_{\text{S}}^{\text{eq}}} \right) \langle \sigma v^2 \rangle_{3s \rightarrow 2s} + \left(\frac{n_{\text{W}}}{n_{\text{S}}^{\text{eq}}} \right)^2 \langle \sigma v \rangle_{\text{S S} \rightarrow \text{W W}}}{\langle \sigma v \rangle_{\text{S S} \rightarrow \text{SM SM}} + n_{\text{S}} \langle \sigma v^2 \rangle_{3s \rightarrow 2s} + \langle \sigma v \rangle_{\text{S S} \rightarrow \text{W W}}} \right]^{1/2} \quad \text{for } m_{\text{S}} > m_{\text{W}}. \quad (3.4)$$

Even larger enhancement of DM conversion compared to the self-annihilation of SIMP, $\gamma_{3s \rightarrow 2s} \lesssim \gamma_{sw}$, gives a completely different scenario, as shown in $\textcircled{\text{IV}}$ of figs. 2c, 2d and by deep blue, brown, light blue lines in figs. 2a, 2b. The conversion rate depends on the conversion cross-section as well as the number density during or before the heavier component freeze out. When the conversion is larger than SIMP self-annihilation, the heavier component continues to deplete into the lighter ones even after decoupling from the thermal bath. Since the lighter component has frozen out before, the heavier component goes into the modified equilibrium; see the light blue dashed line in figs. 2a, 2b. With the enhancement of the conversion cross-section, the number density for lighter one doesn't change much

due to the gradual decrease of heavy particle number density with the enhancement of conversion cross-section, and both simultaneously fix the light particle number density in region (IV) of figs. 2c, 2d. However, here the SIMP is not purely a SIMP as its freeze out is mostly governed by conversion.

4 A model example of pFIMP-SIMP

Let us now discuss a model example of pFIMP-SIMP set up. Here we introduce a real scalar ϕ and a complex scalar singlet field χ as DM components, which are stable under $\mathbb{Z}_2 \otimes \mathbb{Z}_3$ symmetry and charge assignments are shown in tab. 2. The dark sector Lagrangian

Dark Fields	\mathbb{Z}_2	\mathbb{Z}_3
χ	χ	$\omega\chi$ or $\omega^2\chi$
ϕ	$-\phi$	ϕ

Table 2: Dark sector fields (χ and ϕ) and their quantum numbers where $\omega = e^{i2\pi/3}$.

obeying the symmetry can be written as,

$$\begin{aligned} \mathcal{L} = & \mathcal{L}_{\text{SM}} + \mu_H^2 H^\dagger H - \lambda_H (H^\dagger H)^2 + \frac{1}{2} |\partial_\mu \phi|^2 - \frac{1}{2} \mu_\phi^2 \phi^2 - \frac{1}{4!} \lambda_\phi \phi^4 + |\partial_\mu \chi|^2 - \mu_\chi^2 |\chi|^2 \\ & - \lambda_\chi |\chi^* \chi|^2 - \frac{1}{2} \mu_3 (\chi^3 + \chi^{*3}) - \frac{1}{2} \lambda_{\phi H} \phi^2 H^\dagger H - \lambda_{\chi H} |\chi|^2 H^\dagger H - \frac{1}{2} \lambda_{\chi\phi} |\chi|^2 \phi^2. \end{aligned} \quad (4.1)$$

After spontaneous symmetry breaking, $H = \left(0 \frac{v+h}{\sqrt{2}}\right)^T$. From the interactions as in Eq. (4.1), χ having $3 \rightarrow 2$ depletion, can be a SIMP, while ϕ can be pFIMP. Understandably, this is the simplest model example of pFIMP-SIMP set up. We are interested in a small mass (\sim MeV) scale of pFIMP, as the SIMP is validated in that mass range only, as discussed before. We choose small values of Higgs portal coupling $\lambda_{\phi H}$. This helps the pFIMP to remain out of thermal bath, at the same time, helps evading Higgs to invisible branching ratio. We will also choose the other Higgs portal coupling $\lambda_{\chi H}$ to be small as well to adhere to the SIMP limit of χ . This also takes care of the invisible Higgs branching ratio to χ pair.

4.1 Solution of coupled Boltzmann Equation and relic density

Assuming CP conservation existing inside the dark sector, the coupled Boltzmann Equation for two DMs, where $Y_s = Y_\chi + Y_{\chi^*}$ with $Y_\chi = Y_{\chi^*}$ is given by,

$$\begin{aligned} \frac{dY_\phi}{dx} = & \frac{2s}{x \mathcal{H}(x)} \left[\frac{1}{s} \left(Y_h^{\text{eq}} - Y_h^{\text{eq}} \frac{Y_\phi^2}{Y_\phi^{\text{eq}^2}} \right) \langle \Gamma \rangle_{h \rightarrow \phi \phi} + \left(Y_{\text{SM}}^{\text{eq}^2} - Y_{\text{SM}}^{\text{eq}^2} \frac{Y_\phi^2}{Y_\phi^{\text{eq}^2}} \right) \langle \sigma v \rangle_{\text{SM SM} \rightarrow \phi \phi} \right. \\ & \left. + \frac{1}{4} \left(Y_s^2 - Y_s^{\text{eq}^2} \frac{Y_\phi^2}{Y_\phi^{\text{eq}^2}} \right) \langle \sigma v \rangle_{\chi \chi^* \rightarrow \phi \phi} \right], \end{aligned} \quad (4.2)$$

$$\frac{dY_s}{dx} = -\frac{\mathbf{s}}{x \mathcal{H}(x)} \left[\frac{1}{2} (Y_s^2 - Y_s^{\text{eq}^2}) \langle \sigma v \rangle_{\chi \chi^* \rightarrow \text{SM SM}} + \frac{\mathbf{s}}{4} (Y_s^3 - Y_s^2 Y_s^{\text{eq}}) \langle \sigma v^2 \rangle_{3\chi \rightarrow 2\chi} \right. \\ \left. + \frac{1}{2} \left(Y_s^2 - Y_s^{\text{eq}^2} \frac{Y_\phi^2}{Y_\phi^{\text{eq}^2}} \right) \langle \sigma v \rangle_{\chi \chi^* \rightarrow \phi \phi} \right]. \quad (4.3)$$

In the above, $\text{SM} = \{\text{h}, \text{W}^\pm, \text{Z}, \text{leptons}, \text{quarks}\}$, \mathbf{s} represents entropy density, $Y_i^{\text{eq}} = n_i^{\text{eq}}/\mathbf{s}$ is the equilibrium yield of i^{th} particle has mentioned in previous section, and,

$$\langle \sigma v^2 \rangle_{3\chi \rightarrow 2\chi} = 2 \left(\langle \sigma v^2 \rangle_{\chi\chi\chi \rightarrow \chi\chi^*} + \langle \sigma v^2 \rangle_{\chi\chi^* \chi^* \rightarrow \chi\chi} \right).$$

The total relic density is written in terms of DM yields obtained from the solution of cBEQ 4.3, after freeze out,

$$\Omega_{\text{DM}} h^2 = 2.74385 \times 10^8 [m_\chi Y_\chi + m_\phi Y_\phi]_{x \rightarrow \infty}. \quad (4.4)$$

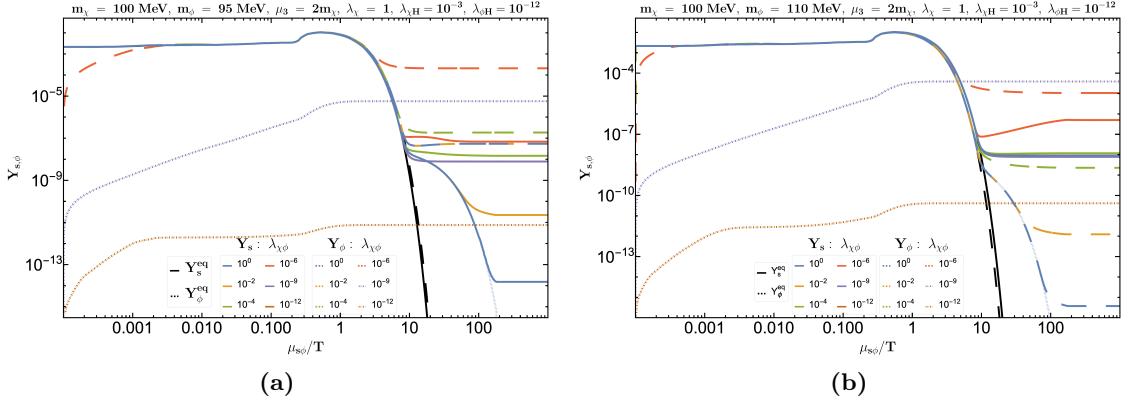


Figure 3: Solution to the cBEQ 4.3, where figs. 3a and 3b represents $m_\chi > m_\phi$ and $m_\chi < m_\phi$ scenarios respectively. The thick, dashed and dotted color lines represent the SIMP, FIMP and pFIMP cases respectively. Different colors show $\lambda_{\chi\phi}$ variation as mentioned in the figure inset. The thick black and dashed lines represent the SIMP and pFIMP equilibrium yields. Other parameter kept fixed are mentioned in the figure heading.

The solution of cBEQ 4.3 provides the yield of SIMP (Y_χ) and pFIMP (Y_ϕ) as shown in fig. 3 with the variation of $\mu_{s\phi}/T$ for different mass hierarchies; fig. 3a shows the case for $m_\chi > m_\phi$ and fig. 3b represents the case for $m_\chi < m_\phi$. The explanation of this figure is similar to that of fig. 2 (top row). The only change here is that we vary the free-parameter $\lambda_{\chi\phi}$ in solving cBEQ instead of choosing a numerical value for the conversion cross-section $\sigma_{\text{SS} \rightarrow \text{WW}}^{\text{T}}$ as done before. For small values of $\lambda_{\chi\phi}$ (10^{-12} , 10^{-9}), ϕ shows pure FIMP like behaviour before freezing-in, as shown by the violet and orange dot-dashed lines in figs for both the mass hierarchies. Enhancement of $\lambda_{\chi\phi}$ ($\sim 10^{-6}$) makes ϕ reach thermal bath and follow the equilibrium distribution before freezing out; ϕ becomes pFIMP here and is represented by dashed red lines in both the figs. At this moment, the number density of SIMP χ is enhanced due to new production channel opening up via conversion.

With further enhancement of $\lambda_{\chi\phi}$ ($\gtrsim 10^{-6} - 10^{-4}$), we observe a decrease in both SIMP and pFIMP number densities, shown by green thick and dashed lines in fig. 3 for both the mass hierarchies. This serve as the ideal pFIMP-SIMP parameter space, where we achieve under abundance for both the DM components. If $\lambda_{\chi\phi}$ is enhanced further to $\sim \{10^{-2}, 10^0\}$ then the annihilation of the heavier DM component to the lighter one is possible even after the freeze out of the lighter component, then the heavier component follows modified equilibrium distribution following eqs. 3.4, and 3.3 before freezing out. The yellow ($\lambda_{\chi\phi} \sim 10^{-2}$) and light blue ($\lambda_{\chi\phi} \sim 10^0$) thick (SIMP) and dashed (pFIMP) lines represent DM yields following such modified distributions.

4.2 Constraints on the model parameter space

We will provide a short account of the results obtained from the parameter space scan here. In the two-component SIMP-pFIMP scenario, total relic density ($\Omega_{\text{DM}}^{\text{obs}}$) is gathered from both SIMP and pFIMP, obtained from the solution of cBEQ in eq. 4.3. In our model, as described by eq. 4.1, free parameters relevant for the cosmological evolution are m_χ , m_ϕ , λ_χ , μ_3 and $\lambda_{\chi\phi}$. Other parameters like $\lambda_{\chi H} \sim 10^{-3}$ and $\lambda_{\phi H} \sim 10^{-12}$ are kept fixed to maintain the criteria of keeping χ as SIMP and ϕ as pFIMP. Also, $\lambda_{\chi H}$ and $\lambda_{\phi H}$ do not play a direct role in the relic density of the DM components. In fig. 4, we have shown a few variations in the parameters space scan.

DM self interaction plays a crucial role here. In the SIMP-pFIMP scenario, DM self-interaction cross-section over DM mass ($\sigma_{\text{self}}/m_{\text{DM}}$) depends not only on their self-scattering cross-sections but also on their individual relic densities, which are restricted by Bullet cluster and Abell cluster observations, see eq C.2. The parameters $\lambda_{\chi H}$ and λ_ϕ play a significant role in DM self-interaction processes. If the pFIMP relic is dominant over SIMP, then σ_{self} mostly depends on the $\sigma_{\phi\phi\rightarrow\phi\phi}$, *i.e.* λ_ϕ , but, in case of dominant SIMP, the self scattering cross-section depends primarily on *i.e.* λ_χ and $\lambda_{\chi H}$ couplings.

In figs. 4a and 4b, we have plotted the relic density allowed parameter space in $m_\chi - \lambda_\chi$ plane for both the mass hierarchies. SIMP is heavier in the left plot, while pFIMP is heavier on the right. The main parameter that is varied here is the coupling relevant for conversion cross-section, *i.e.* $\lambda_{\chi\phi}$, as shown in the colour bar. Other parameters kept fixed are mentioned in figure heading, they are responsible for keeping the SIMP and pFIMP limit intact and respect unitarity, vacuum stability limits. All the scattered points respect relic density constraint. Those in red respect self interaction limit from Bullet cluster, while those in green respect the limit from Abell cluster. When SIMP is heavier (fig. 4a), pFIMP freezes out before and SIMP relic is smaller and has a subdominant contribution to the total relic density due to modified freeze out. In such circumstances, self interaction limit is less constrained for SIMP and allows $\lambda_\chi \sim \times 10^{-2}$. For a lighter SIMP, the constraint is stricter $\lambda_\chi \sim \times 10^{-1}$. $\lambda_\phi \sim 5.25 \times 10^{-2}$ helps the pFIMP to obey self-interaction bound.

In figs. 4c and 4d, we have plotted the relic allowed parameter space in $m_\chi - \mu_3$ planes. Red points respect self interaction limit from Bullet cluster, while those in green respect the limit from Abell cluster. Almost all the points in the full mass range obeys this limit. We further see a correlation between m_χ and μ_3 , roughly following $\mu_3 \geq 2m_\chi$. As before, $\lambda_{\chi\phi}$ is varied as shown in the colour bar. For larger $\lambda_{\chi\phi}$, when pFIMP is heavier (right

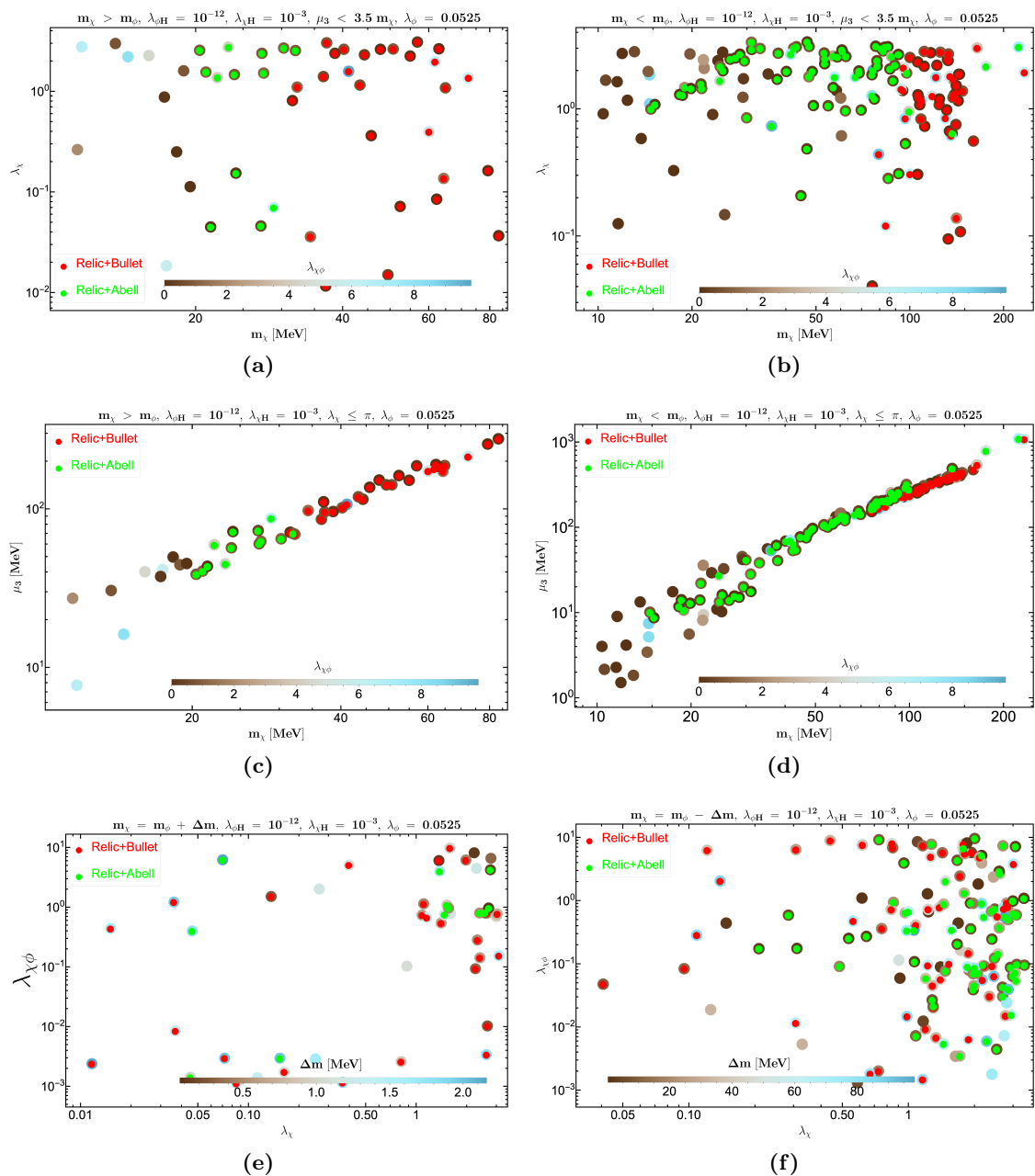


Figure 4: Figs. 4a, 4b and 4c, 4d are represent the DM relic allowed parameter space in $m_\chi - \lambda_\chi$ and $m_\chi - \mu_3$ plane, respectively. The variation of portal coupling $\lambda_{\chi\phi}$ is shown by the Brown-CyanTones color bar. The red and green points represent the points within the Bullet and Abell cluster self-interaction limit. Figs. 4e, 4f represents the relic allowed points in $\lambda_\chi - \lambda_{\chi\phi}$ plane and BrownCyanTones color bar shows the DM mass separation.

hand plot), it shows modified freeze out, and its relic becomes sub-dominant in total DM relic. Under this circumstance, only SIMP self-interaction contributes dominantly to DM self-interaction bound (Note, we kept $\lambda_{\chi H}$ is constant). $\lambda_{\chi H} \sim 10^{-3}$ is preferred for the

allowed parameter space to obey both Bullet and Abell cluster bound while λ_ϕ is free. Lower mass limit $m_\chi \lesssim 15$ MeV is disfavoured from the self interaction limit.

In figs. 4e and 4f, we have shown the relic density allowed points with DM mass variation in the color bar in $\lambda_\chi - \lambda_{\chi\phi}$ plane. As such there is no specific correlation between these parameters to be observed to yield correct relic abundance and self interaction limits. We see that the maximum available DM mass separation is up to 5 MeV for $m_\chi > m_\phi$, but more relaxed (up to 50 MeV) for the opposite mass hierarchy. This is an important result of this pFIMP-SIMP scenario, to agree with the model-independent analysis of pFIMP in the presence of any thermal DM [36, 37].

Before concluding this section, let us briefly summarise the outcome of this analysis. The two-component DM scenario in the presence of SIMP has not been studied much excepting [32, 33]. Here, we have studied pFIMP dynamics in the presence of SIMP that helps a feebly coupled DM to equilibrate to thermal bath and freeze out via substantial interaction with SIMP. The major outcomes of this SIMP-pFIMP analysis are that relic density allowed parameter space of this model surpasses the single component SIMP allowed range, in particular, the SIMP mass is allowed up to ~ 50 MeV when $m_\phi > m_\chi$. Second, DM self-interaction provides the most dominant constraint, in particular, λ_ϕ and $\lambda_{\chi H}$ couplings, which are free parameters in context of DM relic density gets constrained by DM self-interaction bound.

4.3 Detection possibility

The required condition to keep the SIMP in kinematic equilibrium is $\Gamma_{\chi\chi^* \rightarrow f\bar{f}} \lesssim \Gamma_{3\chi \rightarrow 2\chi} \lesssim \Gamma_{\chi f \rightarrow \chi f}$, which has motivated us to choose $\lambda_{\chi H}$ as free parameter (in single component) as long as it doesn't become too high such that the DM DM \rightarrow SM SM annihilation dominates over the self-annihilation. As this parameter is suppressed, it doesn't have a significant role in SIMP freeze out and relic density, but this might be constrained by presently available SIMP-electron scattering bound like XENON1T [68], CRESST-III [69], DAMIC-M [70], DarkSide-50 [71], ALETHEIA [72] and DarkSide-20k [73], LDMX [74] (proposed) etc.

Unfortunately, in the case of our two-component real and complex scalar pFIMP-SIMP model, it is difficult to detect both the components via direct or indirect detection due to small values of $\lambda_{\chi H}$ with detector's low sensitivity as far as the current and immediate future projection goes. The DM-electron cross-section mostly depend upon the mediator mass m_h and Higgs-DM portal coupling $\lambda_{\chi H}$ for SIMP. Apart from small $\lambda_{\chi H}$, the presence of a heavy (\sim GeV) mediator decreases the DM-electron scattering cross-section. As we already know [36, 37], the pFIMP detection is possible only via thermal DM loop-mediated interaction with the visible sector, so the difficulty in SIMP detection transmits to the difficulty in pFIMP searches as well, although low mass pFIMP takes part in electron scattering. The pFIMP-electron scattering cross-section depends upon the parameters $\lambda_{\chi\phi}$, $\lambda_{\chi H}$ and the mediator mass ($m_h \sim 125$ GeV). In the case of MeV DM (SIMP or pFIMP), the DM-electron scattering cross-section significantly suffers from the presence of heavy mediator.

Therefore detection possibility of such a framework emerges under the possibility of a low mediator mass (\sim MeV). For that the model needs to be augmented further. Besides the particle content of two scalar fields contributing to pFIMP-WIMP model, we consider

a vector-like lepton (VLL) ψ with weak hypercharge $Y = -1$ [75, 76], charged under \mathbb{Z}_3 having transformation like $\psi \rightarrow \omega\psi$. For simplicity, one may assume that this VLL fermion only couples to the first right-handed lepton generation to avoid the strong bounds from the lepton flavour-violating process. The newly extended Lagrangian can be written as,

$$\mathcal{L}_\psi = \bar{\psi} [i\gamma^\mu (\partial_\mu + ig'YB_\mu) - m_\psi] \psi - (\mathbf{y}\bar{\psi}e_R\chi + \text{h.c.}) , \quad (4.5)$$

where $g' = (2/v)\sqrt{m_Z^2 - m_W^2}$ is the $U(1)_Y$ gauge coupling. ψ is a vector-like lepton (VLL) with weak hypercharge $Y = -1$ [75, 76] and charged under \mathbb{Z}_3 where transformation is like $\psi \rightarrow \omega\psi$. The perturbative limit on real Yukawa coupling is $\mathbf{y} < \sqrt{4\pi}$ and $m_\psi > m_\chi + m_e$ to ensure the χ stability. The most important mass bound on this charged particle mass comes from LEP [77–81] to be $\gtrsim 103.5$ GeV. In that way, this also becomes a heavy mediator. The detection possibility and phenomenology of such a framework are discussed in [82], with a focus on dark matter masses in the GeV range.

5 Summary and conclusions

Multicomponent DM is a viable option to address observed DM characteristics. Such frameworks can be constituted of any kind of DM particle, like WIMP, FIMP, or SIMP. pFIMP is an interesting possibility which exists only in presence of a thermal DM component, which relies on sizable conversion process to equilibrate with thermal bath and freeze out. In this article, we have discussed pFIMP possibility in presence of SIMP. This is the first kind of an analysis to address such a pFIMP-SIMP framework.

In order to have a clear picture of what two component framework does, we first discuss the simplest SIMP framework, complete analytic solution of SIMP and compare it with the numerical solution using Mathematica to show a close comparison. Notably, this analytical solution does better than the previously obtained one [19] to agree with the numerical solution, which shows the relic density allowed parameter space lies within 10 – 200 MeV of SIMP mass, some portions of which are excluded by the presently available DM self-interaction bound from Bullet and Abell clusters.

To address pFIMP dynamics in presence of SIMP, we first adopt a model independent analysis by solving coupled BEQs, one of which addresses SIMP freeze out, the other pFIMP freeze out. For this part, the responsible thermal average cross-sections are taken as numerical numbers. The solution of cBEQ, as shown in fig. 2, confirms the pFIMP dynamics in the presence of SIMP, when conversion cross-section is varied from feeble to weak strength. We show that a pure FIMP having freeze in can be brought to thermal bath and freeze out when the conversion to accompanying SIMP is sizeable. In pFIMP limit, the depletion within the dark sector $3\text{SIMP} \rightarrow 2\text{SIMP}$ might be comparable to the conversion process $2\text{SIMP} \rightarrow 2\text{pFIMP}$ without affecting the SIMP condition.

In this analysis, we assumed that SM and dark bath are in kinetic equilibrium via elastic scattering of DM with bath particles. This elastic scattering rate measures the momentum exchange rate to/from SM bath from/to the dark sector. If this rate is larger than the Hubble expansion rate, the dark sector and thermal bath are always in kinetic equilibrium,

and both sectors follow the same temperature (bath temperature). This has been validated in the appendix for a typical benchmark. Otherwise, the dark sector temperature would be different from the SM bath. It will be an interesting exercise to take up such an analysis in the context of the SIMP-pFIMP setup.

We next discuss the simplest pFIMP-SIMP model with extension of SM with two scalar singlets (one real, one complex) stabilised by $\mathbb{Z}_2 \otimes \mathbb{Z}_3$ symmetry. We chose the model parameter in such a way that the real scalar behaves as pFIMP (ϕ), while the complex scalar (χ) acts like SIMP. Out of the DM masses, self couplings, portal couplings, and conversion couplings, the conversion coupling $\lambda_{\chi\phi}$ helps the pFIMP reach thermal equilibrium. The parameter space is crucially constrained by the self interaction bounds. Interestingly, couplings like λ_ϕ , and $\lambda_{\chi H}$, which play insignificant role in DM freeze out, gets constrained by DM self-interaction. As usual, DM mass splittings get constrained to yield pFIMP solution, but different depending on mass hierarchy. For example, $\Delta m \lesssim 2$ MeV for heavier SIMP, and $\Delta m \lesssim 100$ MeV when pFIMP is heavier. Also, relic density allowed parameter space of this model surpasses the single component SIMP allowed range, in particular, the SIMP mass is allowed up to ~ 50 MeV when $m_\phi > m_\chi$.

Detectability of pFIMP-SIMP model is difficult as the portal coupling of both pFIMP and SIMP with SM Higgs is suppressed to address their freeze outs. Secondly, their interaction with SM is mediated by SM Higgs, which is way heavier than the DM mass (\sim MeV), making the cross-section further subdued. We thus propose a minimal extension of the dark sector by the inclusion of a charged vector-like lepton. This is primarily assumed to interact with electrons only, to avoid conflicts with lepton flavor violation constraints. This provides a different mediator to interact with direct or indirect searches. The presence of such new Yukawa interaction terms opens up direct (via electron scattering) and indirect (annihilation into electron and photon pair) search prospects of the pFIMP-SIMP scenario.

Acknowledgments

DP thanks Heptagon, IITG, for valuable discussions. SB and JT thanks MTP project at IIT Guwahati, where the work was initiated.

A The semi-analytical solution of a SIMP

The Boltzmann equation for the number density n_s of the SIMP type DM (s),

$$\dot{n}_s + 3Hn_s = - \left(n_s^3 - n_s^2 n_s^{\text{eq}} \right) \langle \sigma v^2 \rangle_{3 \rightarrow 2} - \left(n_s^2 - n_s^{\text{eq}^2} \right) \langle \sigma v \rangle_{\text{ann}}. \quad (\text{A.1})$$

As the necessity condition for SIMP is $\Gamma_{3 \rightarrow 2} \gtrsim \Gamma_{\text{ann}}$ so we can safely neglect the $\langle \sigma v \rangle_{\text{ann}}$ term, and the BEQ becomes.

$$\frac{dY_s}{dx} = - \frac{n_f}{x^5} \left(Y_s^3 - Y_s^2 Y_s^{\text{eq}} \right), \quad (\text{A.2})$$

where $x = m_s/T$, $n_f = \frac{\mathbf{s}^2 x^4}{\mathcal{H}(x)} \langle \sigma v^2 \rangle_{3 \rightarrow 2}$ with s and $\mathcal{H}(x)$ are entropy density and Hubble parameter, respectively. The equilibrium yield of SIMP is given by Maxwell-Boltzmann distribution, as during freeze out SIMP is in the non-relativistic regime, $Y_s^{\text{eq}} = 0.145(g_s/g_\star^s)x^{3/2}e^{-x} =$

$A x^{3/2} e^{-x}$ where $A = 0.145(g_s/g_\star^s)$. Another important assumption is that the entropy and matter degrees of freedom are nearly equal during SIMP freezes out ($x_{\text{FO}} \sim 25$) and constant $g_\star^s \simeq g_\star^\rho \sim 10$.

To solve the BEQ analytically, it would be convenient to divide the whole scenario into three different regions on value of x : **Region I**: $x \ll x_{\text{FO}}$, **Region II**: $x \simeq x_{\text{FO}}$ and **Region III**: $x \gg x_{\text{FO}}$. Let us define the difference of SIMP yield from its equilibrium yield as $\Delta = Y_s - Y_s^{\text{eq}}$ and eq. A.2 becomes,

$$\frac{dY_s^{\text{eq}}}{dx} + \frac{d\Delta}{dx} = -\frac{n_f}{x^5} \Delta (\Delta + Y_s^{\text{eq}})^2. \quad (\text{A.3})$$

- **Region I**

For $x \ll x_{\text{FO}}$, $\frac{d\Delta}{dx}$ is negligible and eq. A.3 becomes,

$$\frac{dY_s^{\text{eq}}}{dx} = -\frac{n_f}{x^5} \Delta (\Delta + Y_s^{\text{eq}})^2. \quad (\text{A.4})$$

- **Region II**

In the vicinity of $x \simeq x_{\text{FO}}$, we may further assume $\Delta = c Y_s^{\text{eq}}(x_{\text{FO}})$ where c is unknown constants whose values are determined by matching the analytical result with the numerical one. Substituting in eq. A.4, we get

$$\left. \frac{dY_s^{\text{eq}}}{dx} \right|_{x=x_{\text{FO}}} = -\frac{n_f}{x_{\text{FO}}^5} c (c+1)^2 Y_s^{\text{eq}^3}(x_{\text{FO}}). \quad (\text{A.5})$$

After simplification, we get,

$$x_{\text{FO}}^2 e^{2x_{\text{FO}}} - \frac{3}{2} x_{\text{FO}} e^{2x_{\text{FO}}} = \underbrace{n_f A^2 c (c+1)^2}_P. \quad (\text{A.6})$$

The solution of eq. A.6 gives us the freeze out point of SIMP is,

$$x_{\text{FO}} \approx \ln \sqrt{P} - \ln \ln \sqrt{P}. \quad (\text{A.7})$$

- **Region III**

When $x \gg x_{\text{FO}}$, then, Y_s^{eq} and $\frac{dY_s^{\text{eq}}}{dx}$ are exponentially suppressed, so, $\Delta \gg Y_s^{\text{eq}}$ and eq. A.3 becomes,

$$\frac{d\Delta}{dx} = -\frac{n_f}{x^5} \Delta^3. \quad (\text{A.8})$$

After solving the differential equation between x_{FO} to x with $\Delta(x) \gg \Delta(x_{\text{FO}})$, we get,

$$\Delta(x) = \left[\frac{1}{\Delta(x_{\text{FO}})^2} - \frac{n_f}{2} \left(\frac{1}{x^4} - \frac{1}{x_{\text{FO}}^4} \right) \right]^{-\frac{1}{2}}. \quad (\text{A.9})$$

Following $\Delta(x_{\text{FO}}) \approx cY_s^{\text{eq}}(x_{\text{FO}})$ at $x = x_{\text{CMB}} = m_s/T_{\text{CMB}}$, the SIMP yields is

$$Y_s(x_{\text{CMB}}) \approx \Delta(x_{\text{CMB}}) \approx \left[\frac{1}{\Delta(x_{\text{FO}})^2} - \frac{n_f}{2} \left(\frac{1}{x_{\text{CMB}}^4} - \frac{1}{x_{\text{FO}}^4} \right) \right]^{-\frac{1}{2}}. \quad (\text{A.10})$$

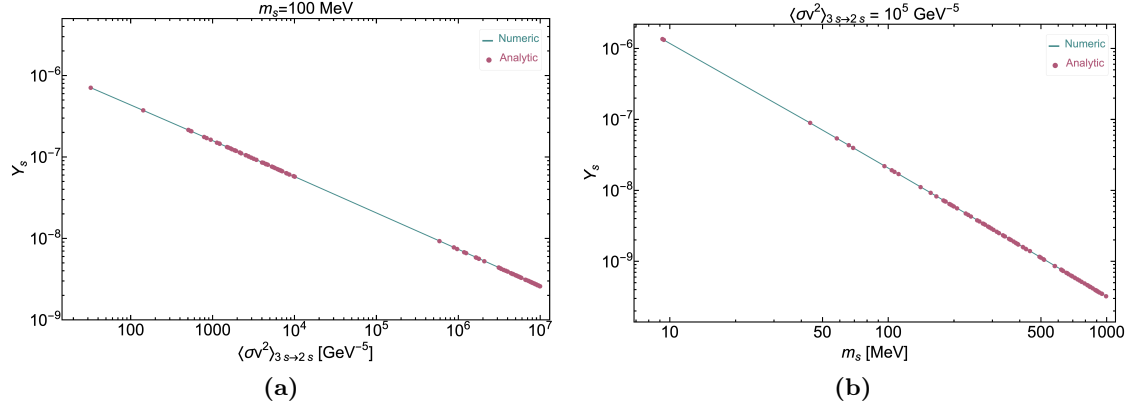


Figure 5: A comparison plot analytic vs numeric solution of BEQ where we have considered $g_*^s = g_*^p = 10.75$, $g_s = 2$ (for complex scalar) and have chosen $c(c+1)^2 = 4.5$.

B Possible Feynman diagrams related to DM phenomenology

We have calculated the squared matrix amplitude for non-relativistic DMs using FeynCalc [83] and CalcHEP [84].

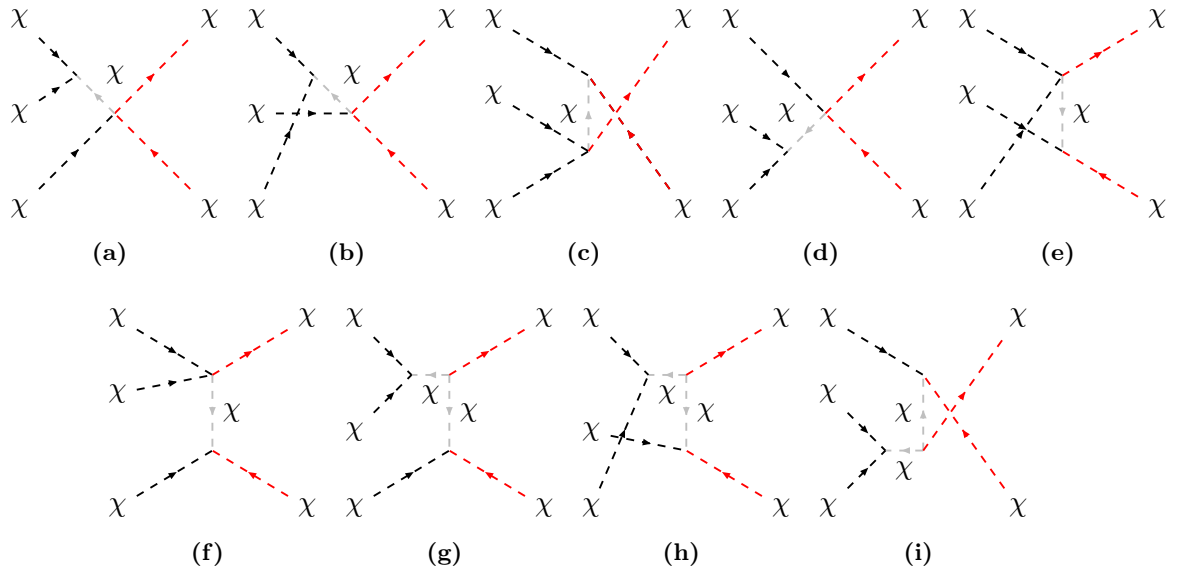


Figure 6: Self annihilation via $\chi(p_1)\chi(p_2)\chi(p_3) \rightarrow \chi(p_4)\chi^*(p_5)$ process.

$$|\overline{\mathcal{M}_6}|^2 = \frac{9\mu_3^2}{4m_\chi^8} \left(4\lambda_\chi m_\chi^2 + 9\mu_3^2\right)^2. \quad (\text{B.1})$$

and

$$\langle \sigma v^2 \rangle_{\chi\chi\chi \rightarrow \chi\chi^*} = \frac{1}{64\pi m_\chi^3} \left(\frac{K_1(m_\chi/T)}{K_2(m_\chi/T)} \right)^3 \frac{\sqrt{5}}{6} |\overline{\mathcal{M}_{\chi\chi\chi \rightarrow \chi\chi^*}}|^2. \quad (\text{B.2})$$

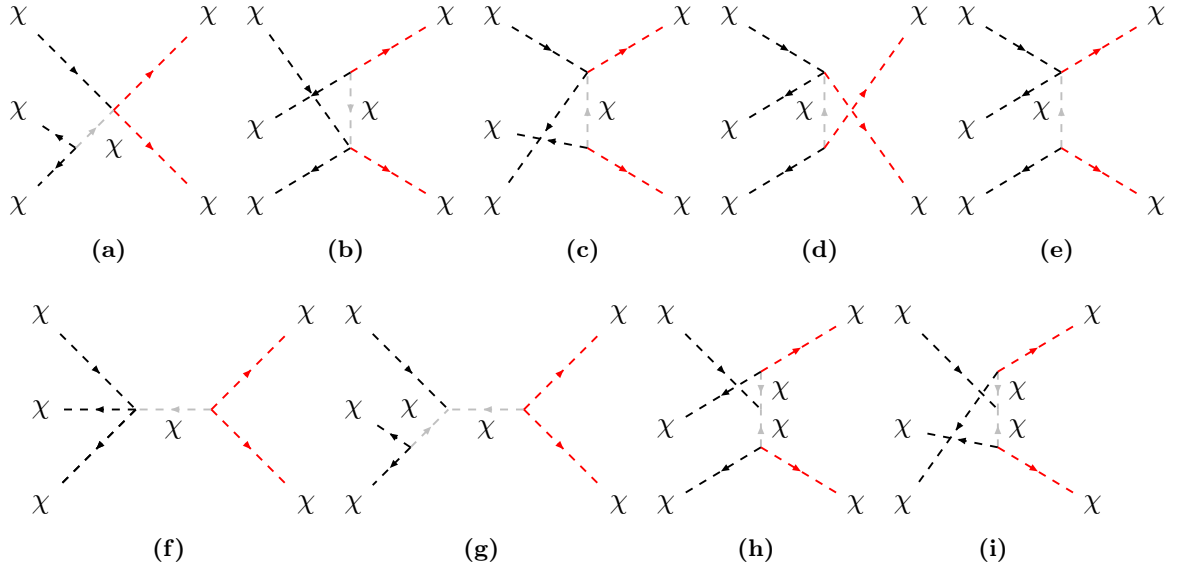


Figure 7: Self-annihilation of SIMP via $\chi\chi^*\chi^* \rightarrow \chi\chi$ process.

$$|\overline{\mathcal{M}_7}|^2 = \frac{\mu_3^2}{64m_\chi^8} \left(117\mu_3^2 - 148\lambda_\chi m_\chi^2\right)^2. \quad (\text{B.3})$$

and

$$\langle \sigma v^2 \rangle_{\chi\chi^*\chi^* \rightarrow \chi\chi} = \frac{1}{64\pi m_\chi^3} \left(\frac{K_1(m_\chi/T)}{K_2(m_\chi/T)} \right)^3 \frac{\sqrt{5}}{6} |\overline{\mathcal{M}_{\chi\chi^*\chi^* \rightarrow \chi\chi}}|^2. \quad (\text{B.4})$$

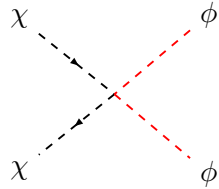


Figure 8: Conversion of SIMP to pFIMP via $\chi\chi^* \rightarrow \phi\phi$ process.

C Dark Matter self-interaction

In single component complex scalar SIMP scenario, The effective DM self-scattering cross-section over mass is written as [41],

$$\frac{\sigma_{\text{self}}}{m_{\text{DM}}} = \frac{1}{m_{\chi}} \left(\frac{\Omega_{\chi}^2}{\Omega_{\text{DM}}^2} \sigma_{\chi\chi \rightarrow \chi\chi} + \frac{\Omega_{\chi^*}^2}{\Omega_{\text{DM}}^2} \sigma_{\chi^* \chi^* \rightarrow \chi^* \chi^*} + \frac{\Omega_{\chi}}{\Omega_{\text{DM}}} \frac{\Omega_{\chi^*}}{\Omega_{\text{DM}}} \sigma_{\chi\chi^* \rightarrow \chi\chi^*} \right). \quad (\text{C.1})$$

In the multicomponent scenario, we take DM mass as effective m_{DM} weighted by effective

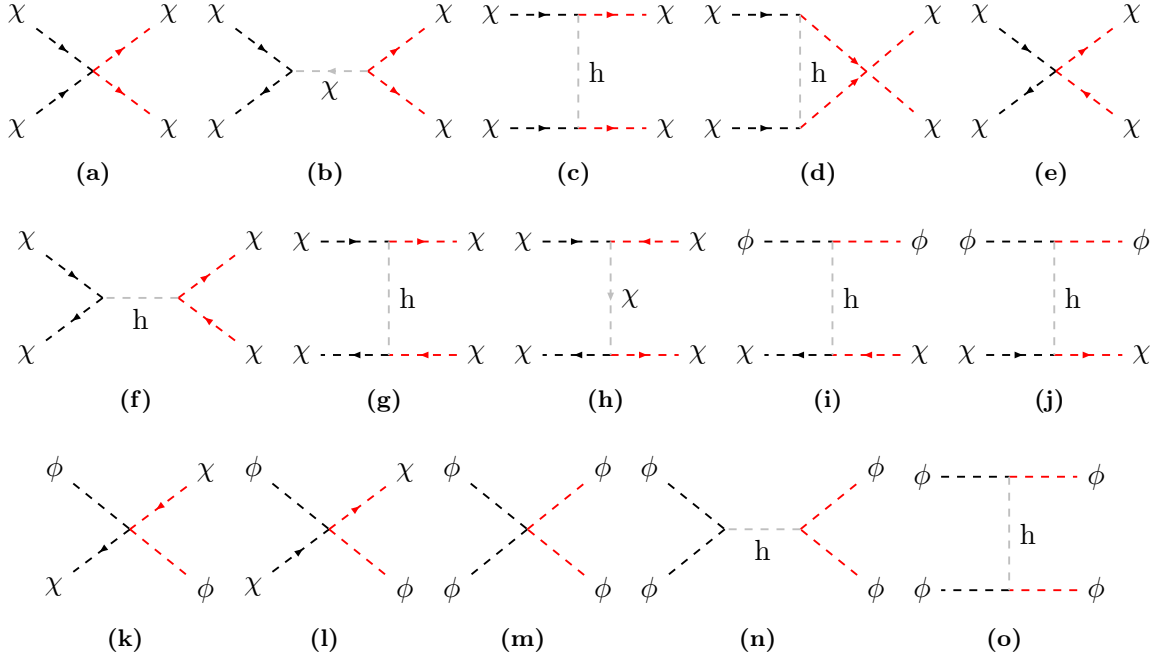


Figure 9: Dark matter self scattering

relic contribution for a particular DM and the analytic expression could be written as [33],

$$\begin{aligned} \frac{\sigma_{\text{self}}}{m_{\text{DM}}} = & \left(\frac{\Omega_{\chi}}{\Omega_{\text{DM}}} \right)^2 \frac{1}{m_{\chi}} \left(\sigma_{\chi\chi \rightarrow \chi\chi} + \sigma_{\chi^* \chi^* \rightarrow \chi^* \chi^*} + \sigma_{\chi\chi^* \rightarrow \chi\chi^*} + \sigma_{\chi\chi^* \rightarrow \phi\phi} \right) \\ & + \left(\frac{\Omega_{\phi}}{\Omega_{\text{DM}}} \right)^2 \frac{1}{m_{\phi}} \sigma_{\phi\phi \rightarrow \phi\phi} + \frac{\Omega_{\chi}}{\Omega_{\text{DM}}} \frac{\Omega_{\phi}}{\Omega_{\text{DM}}} \frac{2}{m_{\chi} + m_{\phi}} \left(\sigma_{\phi\chi \rightarrow \phi\chi} + \sigma_{\phi\chi^* \rightarrow \phi\chi^*} \right). \end{aligned} \quad (\text{C.2})$$

where,

$$\sigma_{\chi\chi\rightarrow\chi\chi} = \frac{1}{16\pi(m_\chi + m_\chi)^2} \left(|\mathcal{M}_{\chi\chi\rightarrow\chi\chi}|^2 + |\mathcal{M}_{\chi^*\chi^*\rightarrow\chi^*\chi^*}|^2 \right), \quad (\text{C.3})$$

$$\sigma_{\chi\chi^*\rightarrow\chi\chi^*} = \frac{1}{16\pi(m_\chi + m_{\chi^*})^2} |\mathcal{M}_{\chi\chi^*\rightarrow\chi\chi^*}|^2, \quad (\text{C.4})$$

$$\sigma_{\chi\chi^*\rightarrow\phi\phi} = \frac{1}{16\pi(m_\chi + m_{\chi^*})^2} |\mathcal{M}_{\chi\chi^*\rightarrow\phi\phi}|^2, \quad (\text{C.5})$$

$$\sigma_{\phi\phi\rightarrow\phi\phi} = \frac{1}{16\pi(m_\phi + m_\phi)^2} |\mathcal{M}_{\phi\phi\rightarrow\phi\phi}|^2, \quad (\text{C.6})$$

$$\sigma_{\phi\chi\rightarrow\phi\chi} = \frac{1}{16\pi(m_\phi + m_\chi)^2} \left(|\mathcal{M}_{\phi\chi\rightarrow\phi\chi}|^2 + |\mathcal{M}_{\phi\chi^*\rightarrow\phi\chi^*}|^2 \right), \quad (\text{C.7})$$

with,

$$|\mathcal{M}_{\chi\chi\rightarrow\chi\chi}|^2 = \frac{\left(m_h^2(3\mu_3^2 + 4\lambda_\chi m_\chi^2) - 2\lambda_{\chi H}^2 v^2 m_\chi^2 \right)^2}{2m_\chi^4 m_h^4}, \quad (\text{C.8})$$

$$|\mathcal{M}_{\chi\chi^*\rightarrow\chi\chi^*}|^2 = \frac{\left(m_h^2(4m_\chi^2 - m_h^2)(9\mu_3^2 - 4\lambda_\chi m_\chi^2) - 2\lambda_{\chi H}^2 v^2 m_\chi^2 (m_h^2 - 2m_\chi^2) \right)^2}{m_\chi^4 m_h^4 (m_h^2 - 4m_\chi^2)^2}, \quad (\text{C.9})$$

$$|\mathcal{M}_{\chi\chi^*\rightarrow\phi\phi}|^2 = \frac{\left(4\lambda_{\chi\phi} m_\chi^2 - \lambda_{\chi\phi} m_h^2 + \lambda_{\chi H} \lambda_{\phi H} v^2 \right)^2}{2(m_h^2 - 4m_\chi^2)^2}, \quad (\text{C.10})$$

$$|\mathcal{M}_{\chi\phi\rightarrow\chi\phi}|^2 = \frac{\left(\lambda_{\chi\phi} \left((m_\chi - m_\phi)^2 - m_h^2 \right) - \lambda_{\chi H} \lambda_{\phi H} v^2 \right)^2}{\left((m_\chi - m_\phi)^2 - m_h^2 \right)^2}, \quad (\text{C.11})$$

$$|\mathcal{M}_{\phi\phi\rightarrow\phi\phi}|^2 = \frac{\left(\lambda_\phi (m_h^4 - 4m_h^2 m_\phi^2) + \lambda_{\phi H}^2 (8m_\phi^2 - 3m_h^2) v^2 \right)^2}{2m_h^4 (m_h^2 - 4m_\phi^2)^2}. \quad (\text{C.12})$$

and $\Omega_\chi = \Omega_s/2$, $\Omega_{\text{DM}} = \Omega_s + \Omega_\phi$.

D DM Kinetic equilibration

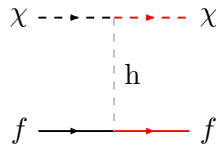


Figure 10: The Feynman diagram represent the DM (χ) and SM fermions (f) scattering.

We already discussed that the kinetic equilibrium of SIMP with SM is achieved after considering an appropriate choice of portal coupling. Only relativistic fermions are available during SIMP freezes-out, and contributing to kinetic decoupling condition is written

regarding DM-SM scattering, fig. 10, rate as,

$$2 \sum_f \Gamma_{\chi f \rightarrow \chi \rightarrow f} = 2 \sum_f \langle \sigma v \rangle_{\chi f \rightarrow \chi f} n_f^{\text{eq}}(T) \gtrsim \mathcal{H}(T). \quad (\text{D.1})$$

where,

$$\langle \sigma v \rangle_{\chi f \rightarrow \chi f} = \frac{\int_{(m_\chi + m_f)^2}^{\infty} \sigma_{\chi f \rightarrow \chi f} K_1 \left(\frac{\sqrt{s}}{T} \right) \sqrt{s - (m_\chi - m_f)^2} \left(s - (m_\chi + m_f)^2 \right) ds}{8T m_\chi^2 m_f^2 K_2 \left(\frac{m_\chi}{T} \right) K_2 \left(\frac{m_f}{T} \right)}. \quad (\text{D.2})$$

and two factors come from SM fermion and anti-fermion contribution. Fig. 11 represents

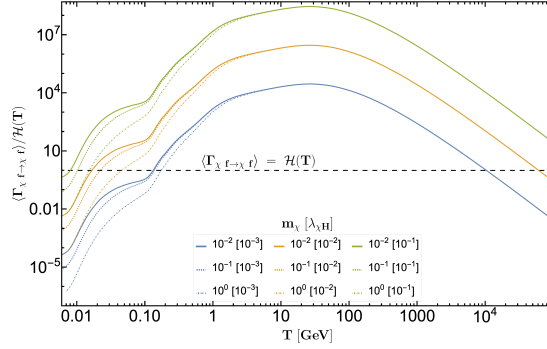


Figure 11: The evaluation of DM (χ)-fermion elastic scattering rate with temperature. The different color lines represent the different m_χ masses in the GeV unit, and coupling is mentioned in the figure inset.

the evolution of DM-SM elastic scattering rate with the SM bath temperature (T). Our work focuses on sub-MeV DMs and suitable choice of $\lambda_{\chi H} \sim 0.1$, without affecting DM relic, to achieve kinetic equilibrium between DM and SM bath.

The kinetic equilibration, with thermal bath, of χ ensures the pFIMP (ϕ) kinetic equilibration also because of the presence of strong self-interaction among themselves. For this reason, there is no necessity to do similar kinds of analysis for ϕ .

References

- [1] F. Zwicky, *On the Masses of Nebulae and of Clusters of Nebulae*, *Astrophys. J.* **86** (1937) 217.
- [2] F. Zwicky, *Die Rotverschiebung von extragalaktischen Nebeln*, *Helv. Phys. Acta* **6** (1933) 110.
- [3] Y. Sofue and V. Rubin, *Rotation curves of spiral galaxies*, *Ann. Rev. Astron. Astrophys.* **39** (2001) 137 [[astro-ph/0010594](#)].
- [4] E. Hayashi and S.D.M. White, *How Rare is the Bullet Cluster?*, *Mon. Not. Roy. Astron. Soc.* **370** (2006) L38 [[astro-ph/0604443](#)].
- [5] WMAP SCIENCE TEAM collaboration, *Results from the Wilkinson Microwave Anisotropy Probe*, *PTEP* **2014** (2014) 06B102 [[1404.5415](#)].
- [6] PLANCK collaboration, *Planck 2018 results. VI. Cosmological parameters*, *Astron. Astrophys.* **641** (2020) A6 [[1807.06209](#)].
- [7] D. Clowe, M. Bradac, A.H. Gonzalez, M. Markevitch, S.W. Randall, C. Jones et al., *A direct empirical proof of the existence of dark matter*, *Astrophys. J. Lett.* **648** (2006) L109 [[astro-ph/0608407](#)].
- [8] L. Roszkowski, E.M. Sessolo and S. Trojanowski, *WIMP dark matter candidates and searches—current status and future prospects*, *Rept. Prog. Phys.* **81** (2018) 066201 [[1707.06277](#)].
- [9] M. Kamionkowski and M.S. Turner, *THERMAL RELICS: DO WE KNOW THEIR ABUNDANCES?*, *Phys. Rev. D* **42** (1990) 3310.
- [10] P. Gondolo and G. Gelmini, *Cosmic abundances of stable particles: Improved analysis*, *Nucl. Phys. B* **360** (1991) 145.
- [11] G. Jungman, M. Kamionkowski and K. Griest, *Supersymmetric dark matter*, *Phys. Rept.* **267** (1996) 195 [[hep-ph/9506380](#)].
- [12] J. Edsjo and P. Gondolo, *Neutralino relic density including coannihilations*, *Phys. Rev. D* **56** (1997) 1879 [[hep-ph/9704361](#)].
- [13] A. Bottino, V. de Alfaro, N. Fornengo, G. Mignola and M. Pignone, *On the neutralino as dark matter candidate. 1. Relic abundance.*, *Astropart. Phys.* **2** (1994) 67 [[hep-ph/9309218](#)].
- [14] Y. Hochberg, E. Kuflik, T. Volansky and J.G. Wacker, *Mechanism for Thermal Relic Dark Matter of Strongly Interacting Massive Particles*, *Phys. Rev. Lett.* **113** (2014) 171301 [[1402.5143](#)].
- [15] Y. Hochberg, E. Kuflik, H. Murayama, T. Volansky and J.G. Wacker, *Model for Thermal Relic Dark Matter of Strongly Interacting Massive Particles*, *Phys. Rev. Lett.* **115** (2015) 021301 [[1411.3727](#)].
- [16] Y. Hochberg, E. Kuflik and H. Murayama, *SIMP Spectroscopy*, *JHEP* **05** (2016) 090 [[1512.07917](#)].
- [17] S. Tulin and H.-B. Yu, *Dark Matter Self-interactions and Small Scale Structure*, *Phys. Rept.* **730** (2018) 1 [[1705.02358](#)].
- [18] S.-M. Choi, H.M. Lee, P. Ko and A. Natale, *Resolving phenomenological problems with strongly-interacting-massive-particle models with dark vector resonances*, *Phys. Rev. D* **98** (2018) 015034 [[1801.07726](#)].

- [19] S. Bhattacharya, P. Ghosh and S. Verma, *SIMPler realisation of Scalar Dark Matter*, *JCAP* **01** (2020) 040 [[1904.07562](#)].
- [20] B. Barman and N. Bernal, *Gravitational SIMPs*, *JCAP* **06** (2021) 011 [[2104.10699](#)].
- [21] A. Kamada, S. Kobayashi and T. Kuwahara, *Perturbative unitarity of strongly interacting massive particle models*, *JHEP* **02** (2023) 217 [[2210.01393](#)].
- [22] L.J. Hall, K. Jedamzik, J. March-Russell and S.M. West, *Freeze-In Production of FIMP Dark Matter*, *JHEP* **03** (2010) 080 [[0911.1120](#)].
- [23] C.E. Yaguna, *The Singlet Scalar as FIMP Dark Matter*, *JHEP* **08** (2011) 060 [[1105.1654](#)].
- [24] N. Bernal, M. Heikinheimo, T. Tenkanen, K. Tuominen and V. Vaskonen, *The Dawn of FIMP Dark Matter: A Review of Models and Constraints*, *Int. J. Mod. Phys. A* **32** (2017) 1730023 [[1706.07442](#)].
- [25] F. D’Eramo and A. Lenoci, *Lower mass bounds on FIMP dark matter produced via freeze-in*, *JCAP* **10** (2021) 045 [[2012.01446](#)].
- [26] N. Chakrabarty, P. Konar, R. Roshan and S. Show, *Thermally corrected masses and freeze-in dark matter: A case study*, *Phys. Rev. D* **107** (2023) 035021 [[2206.02233](#)].
- [27] A. Biswas and A. Gupta, *Calculation of Momentum Distribution Function of a Non-thermal Fermionic Dark Matter*, *JCAP* **03** (2017) 033 [[1612.02793](#)].
- [28] S. Bhattacharya, A. Drozd, B. Grzadkowski and J. Wudka, *Two-Component Dark Matter*, *JHEP* **10** (2013) 158 [[1309.2986](#)].
- [29] S. Bhattacharya, P. Poulose and P. Ghosh, *Multipartite Interacting Scalar Dark Matter in the light of updated LUX data*, *JCAP* **04** (2017) 043 [[1607.08461](#)].
- [30] M. Pandey, D. Majumdar and K.P. Modak, *Two Component Feebly Interacting Massive Particle (FIMP) Dark Matter*, *JCAP* **06** (2018) 023 [[1709.05955](#)].
- [31] S. Peyman Zakeri, S. Mohammad Moosavi Nejad, M. Zakeri and S. Yaser Ayazi, *A Minimal Model For Two-Component FIMP Dark Matter: A Basic Search*, *Chin. Phys. C* **42** (2018) 073101 [[1801.09115](#)].
- [32] S.-Y. Ho, P. Ko and C.-T. Lu, *Scalar and fermion two-component SIMP dark matter with an accidental \mathbb{Z}_4 symmetry*, *JHEP* **03** (2022) 005 [[2201.06856](#)].
- [33] S.-M. Choi, J. Kim, P. Ko and J. Li, *A multi-component SIMP model with $U(1)_X \rightarrow \mathbb{Z}_2 \times \mathbb{Z}_3$* , *JHEP* **09** (2021) 028 [[2103.05956](#)].
- [34] A. Dutta Banik, M. Pandey, D. Majumdar and A. Biswas, *Two component WIMP-FIMP dark matter model with singlet fermion, scalar and pseudo scalar*, *Eur. Phys. J. C* **77** (2017) 657 [[1612.08621](#)].
- [35] S. Bhattacharya, S. Chakraborti and D. Pradhan, *Electroweak symmetry breaking and WIMP-FIMP dark matter*, *JHEP* **07** (2022) 091 [[2110.06985](#)].
- [36] S. Bhattacharya, J. Lahiri and D. Pradhan, *Dynamics of the pseudo-FIMP in presence of a thermal Dark Matter*, *Phys. Rev. D* **108** (2023) L111702 [[2212.07622](#)].
- [37] S. Bhattacharya, J. Lahiri and D. Pradhan, *Detection possibility of a Pseudo-FIMP in presence of a thermal WIMP*, [2212.14846](#).
- [38] S. Bhattacharya, L. Kolay and D. Pradhan, *Multiparticle scalar dark matter with \mathbb{Z}_N symmetry*, [2410.16275](#).

- [39] N. Bernal and X. Chu, Z_2 SIMP Dark Matter, *JCAP* **01** (2016) 006 [[1510.08527](#)].
- [40] H.M. Lee and M.-S. Seo, Communication with SIMP dark mesons via Z' -portal, *Phys. Lett. B* **748** (2015) 316 [[1504.00745](#)].
- [41] S.-M. Choi and H.M. Lee, SIMP dark matter with gauged Z_3 symmetry, *JHEP* **09** (2015) 063 [[1505.00960](#)].
- [42] K. Griest and M. Kamionkowski, Unitarity Limits on the Mass and Radius of Dark Matter Particles, *Phys. Rev. Lett.* **64** (1990) 615.
- [43] D. Bhatia and S. Mukhopadhyay, Unitarity limits on thermal dark matter in (non-)standard cosmologies, *JHEP* **03** (2021) 133 [[2010.09762](#)].
- [44] L. Hui, Unitarity bounds and the cuspy halo problem, *Phys. Rev. Lett.* **86** (2001) 3467 [[astro-ph/0102349](#)].
- [45] M.H. Namjoo, T.R. Slatyer and C.-L. Wu, Enhanced n -body annihilation of dark matter and its indirect signatures, *JHEP* **03** (2019) 077 [[1810.09455](#)].
- [46] R.N. Lerner and J. McDonald, Gauge singlet scalar as inflaton and thermal relic dark matter, *Phys. Rev. D* **80** (2009) 123507 [[0909.0520](#)].
- [47] G. Belanger, K. Kannike, A. Pukhov and M. Raidal, Z_3 Scalar Singlet Dark Matter, *JCAP* **01** (2013) 022 [[1211.1014](#)].
- [48] B.W. Lee, C. Quigg and H.B. Thacker, Weak Interactions at Very High-Energies: The Role of the Higgs Boson Mass, *Phys. Rev. D* **16** (1977) 1519.
- [49] J. Horejsi and M. Kladiva, Tree-unitarity bounds for THDM Higgs masses revisited, *Eur. Phys. J. C* **46** (2006) 81 [[hep-ph/0510154](#)].
- [50] A. Hektor, A. Hryczuk and K. Kannike, Improved bounds on Z_3 singlet dark matter, *JHEP* **03** (2019) 204 [[1901.08074](#)].
- [51] F.C. Adams, General solutions for tunneling of scalar fields with quartic potentials, *Phys. Rev. D* **48** (1993) 2800 [[hep-ph/9302321](#)].
- [52] E.D. Carlson, M.E. Machacek and L.J. Hall, Self-interacting dark matter, *Astrophys. J.* **398** (1992) 43.
- [53] S.-M. Choi, Y. Hochberg, E. Kuflik, H.M. Lee, Y. Mambrini, H. Murayama et al., Vector SIMP dark matter, *JHEP* **10** (2017) 162 [[1707.01434](#)].
- [54] N. Bernal, C. Garcia-Cely and R. Rosenfeld, WIMP and SIMP Dark Matter from the Spontaneous Breaking of a Global Group, *JCAP* **04** (2015) 012 [[1501.01973](#)].
- [55] N. Bernal, X. Chu, C. Garcia-Cely, T. Hambye and B. Zaldivar, Production Regimes for Self-Interacting Dark Matter, *JCAP* **03** (2016) 018 [[1510.08063](#)].
- [56] D.N. Spergel and P.J. Steinhardt, Observational evidence for selfinteracting cold dark matter, *Phys. Rev. Lett.* **84** (2000) 3760 [[astro-ph/9909386](#)].
- [57] D. Clowe, A. Gonzalez and M. Markevitch, Weak lensing mass reconstruction of the interacting cluster 1E0657-558: Direct evidence for the existence of dark matter, *Astrophys. J.* **604** (2004) 596 [[astro-ph/0312273](#)].
- [58] M. Markevitch, A.H. Gonzalez, D. Clowe, A. Vikhlinin, L. David, W. Forman et al., Direct constraints on the dark matter self-interaction cross-section from the merging galaxy cluster 1E0657-56, *Astrophys. J.* **606** (2004) 819 [[astro-ph/0309303](#)].

- [59] S.W. Randall, M. Markevitch, D. Clowe, A.H. Gonzalez and M. Bradac, *Constraints on the Self-Interaction Cross-Section of Dark Matter from Numerical Simulations of the Merging Galaxy Cluster 1E 0657-56*, *Astrophys. J.* **679** (2008) 1173 [0704.0261].
- [60] F. Kahlhoefer, K. Schmidt-Hoberg, J. Kummer and S. Sarkar, *On the interpretation of dark matter self-interactions in Abell 3827*, *Mon. Not. Roy. Astron. Soc.* **452** (2015) L54 [1504.06576].
- [61] A.H.G. Peter, M. Rocha, J.S. Bullock and M. Kaplinghat, *Cosmological Simulations with Self-Interacting Dark Matter II: Halo Shapes vs. Observations*, *Mon. Not. Roy. Astron. Soc.* **430** (2013) 105 [1208.3026].
- [62] M. Rocha, A.H.G. Peter, J.S. Bullock, M. Kaplinghat, S. Garrison-Kimmel, J. Onorbe et al., *Cosmological Simulations with Self-Interacting Dark Matter I: Constant Density Cores and Substructure*, *Mon. Not. Roy. Astron. Soc.* **430** (2013) 81 [1208.3025].
- [63] K.M. Nollett and G. Steigman, *BBN And The CMB Constrain Light, Electromagnetically Coupled WIMPs*, *Phys. Rev. D* **89** (2014) 083508 [1312.5725].
- [64] M. Battaglieri et al., *US Cosmic Visions: New Ideas in Dark Matter 2017: Community Report*, in *U.S. Cosmic Visions: New Ideas in Dark Matter*, 7, 2017 [1707.04591].
- [65] G. Krnjaic and S.D. McDermott, *Implications of BBN Bounds for Cosmic Ray Upscattered Dark Matter*, *Phys. Rev. D* **101** (2020) 123022 [1908.00007].
- [66] P.F. Depta, M. Hufnagel, K. Schmidt-Hoberg and S. Wild, *BBN constraints on the annihilation of MeV-scale dark matter*, *JCAP* **04** (2019) 029 [1901.06944].
- [67] C. Giovanetti, M. Lisanti, H. Liu and J.T. Ruderman, *Joint Cosmic Microwave Background and Big Bang Nucleosynthesis Constraints on Light Dark Sectors with Dark Radiation*, *Phys. Rev. Lett.* **129** (2022) 021302 [2109.03246].
- [68] XENON collaboration, *Light Dark Matter Search with Ionization Signals in XENON1T*, *Phys. Rev. Lett.* **123** (2019) 251801 [1907.11485].
- [69] CRESST collaboration, *First results from the CRESST-III low-mass dark matter program*, *Phys. Rev. D* **100** (2019) 102002 [1904.00498].
- [70] DAMIC-M collaboration, *First Constraints from DAMIC-M on Sub-GeV Dark-Matter Particles Interacting with Electrons*, 2302.02372.
- [71] DARKSIDE collaboration, *Low-Mass Dark Matter Search with the DarkSide-50 Experiment*, *Phys. Rev. Lett.* **121** (2018) 081307 [1802.06994].
- [72] J. Liao, Y. Gao, Z. Liang, Z. Ouyang, Z. Peng, L. Zhang et al., *Introduction to a low-mass dark matter project, ALETHEIA: A Liquid hELium Time projection cHambEr In dArk matter*, 2203.07901.
- [73] DARKSIDE-20K collaboration, *DarkSide-20k: A 20 tonne two-phase LAr TPC for direct dark matter detection at LNGS*, *Eur. Phys. J. Plus* **133** (2018) 131 [1707.08145].
- [74] LDMX collaboration, *Light Dark Matter eXperiment (LDMX)*, 1808.05219.
- [75] P. Athron, C. Balázs, D.H.J. Jacob, W. Kotlarski, D. Stöckinger and H. Stöckinger-Kim, *New physics explanations of a_μ in light of the FNAL muon $g - 2$ measurement*, *JHEP* **09** (2021) 080 [2104.03691].
- [76] J. Kawamura, S. Okawa and Y. Omura, *Current status and muon $g - 2$ explanation of lepton portal dark matter*, *JHEP* **08** (2020) 042 [2002.12534].

- [77] L3 collaboration, *Search for heavy neutral and charged leptons in e^+e^- annihilation at LEP*, *Phys. Lett. B* **517** (2001) 75 [[hep-ex/0107015](#)].
- [78] ALEPH collaboration, *Absolute lower limits on the masses of selectrons and sneutrinos in the MSSM*, *Phys. Lett. B* **544** (2002) 73 [[hep-ex/0207056](#)].
- [79] OPAL collaboration, *Search for anomalous production of dilepton events with missing transverse momentum in e^+e^- collisions at $s^{*(1/2)} = 183\text{-GeV}$ to 209-GeV* , *Eur. Phys. J. C* **32** (2004) 453 [[hep-ex/0309014](#)].
- [80] DELPHI collaboration, *Searches for supersymmetric particles in e^+e^- collisions up to 208-GeV and interpretation of the results within the MSSM*, *Eur. Phys. J. C* **31** (2003) 421 [[hep-ex/0311019](#)].
- [81] L3 collaboration, *Search for scalar leptons and scalar quarks at LEP*, *Phys. Lett. B* **580** (2004) 37 [[hep-ex/0310007](#)].
- [82] J. Lahiri, D. Pradhan and A. Sarkar, *The Influence of Lepton Portal on the WIMP-pFIMP framework*, [2410.19734](#).
- [83] V. Shtabovenko, R. Mertig and F. Orellana, *FeynCalc 10: Do multiloop integrals dream of computer codes?*, [2312.14089](#).
- [84] A. Belyaev, N.D. Christensen and A. Pukhov, *CalcHEP 3.4 for collider physics within and beyond the Standard Model*, *Comput. Phys. Commun.* **184** (2013) 1729 [[1207.6082](#)].